INTERNATIONAL JOURNAL FOR NUMERICAL METHODS IN FLUIDS
Int. J. Numer. Meth. Fluids 2008; **58**:709–725
Published online 14 April 2008 in Wiley InterScience (www.interscience.wiley.com). DOI: 10.1002/fld.1665

A spectral projection method for the analysis of autocorrelation functions and projection errors in discrete particle simulation

André Kaufmann[1,*,†] and Mathieu Moreau[2]

[1]*CERFACS, 42 Av. G. Coriolis, 31057 Toulouse, France*
[2]*IMFT UMR 5502 CNRS/INPT/UPS, Toulouse, France*

SUMMARY

Discrete particle simulation is a well-established tool for the simulation of particles and droplets suspended in turbulent flows of academic and industrial applications. The study of some properties such as the preferential concentration of inertial particles in regions of high shear and low vorticity requires the computation of autocorrelation functions. This can be a tedious task as the discrete point particles need to be projected in some manner to obtain the continuous autocorrelation functions.

Projection of particle properties on to a computational grid, for instance, the grid of the carrier phase, is furthermore an issue when quantities such as particle concentrations are to be computed or source terms between the carrier phase and the particles are exchanged. The errors committed by commonly used projection methods are often unknown and are difficult to analyse. Grid and sampling size limit the possibilities in terms of precision per computational cost.

Here, we present a spectral projection method that is not affected by sampling issues and addresses all of the above issues. The technique is only limited by computational resources and is easy to parallelize. The only visible drawback is the limitation to simple geometries and therefore limited to academic applications.

The spectral projection method consists of a discrete Fourier-transform of the particle locations. The Fourier-transformed particle number density and momentum fields can then be used to compute the autocorrelation functions and the continuous physical space fields for the evaluation of the projection methods error. The number of Fourier components used to discretize the projector kernel can be chosen such that the corresponding characteristic length scale is as small as needed. This allows to study the phenomena of particle motion, for example, in a region of preferential concentration that may be smaller than the cell size of the carrier phase grid.

The precision of the spectral projection method depends, therefore, only on the number of Fourier modes considered. Copyright © 2008 John Wiley & Sons, Ltd.

Received 14 February 2007; Revised 29 September 2007; Accepted 9 October 2007

KEY WORDS: discrete particle simulation; projection method; error analysis; Fourier analysis; interpolation; autocorrelation

*Correspondence to: André Kaufmann, CERFACS, 42 Av. G. Coriolis, 31057 Toulouse, France.
†E-mail: AndreKaufmann@gmx.net, andre.kaufmann@siemens.com

INTRODUCTION

Discrete particle simulation (DPS) is presently the best method to analyse the motion of a large number of particles or droplets interacting with a turbulent carrier phase. Particle collective features, such as particle number densities, are of interest when analysing preferential concentration that occurs in regions of high shear and low vorticity [1]. The study of such features usually involves the computation of correlation functions that can be difficult to evaluate. Here, we propose a computational method for the evaluation of autocorrelation functions for the academic cases of periodic domains commonly used when studying particles in homogeneous isotropic turbulence.

The method is based on a discrete Fourier transform using the particle locations. Therefore, the method does not require a projection on a computational grid. In this method rather a grid in spectral space is used to store the corresponding Fourier modes.

As a coproduct of the method one obtains the Fourier transforms of number density field and momentum fields. Using the inverse Fourier transform, continuous fields of particle number density and particle momentum can be obtained.

The interpolation of the carrier phase to the particle locations has been studied for the computation of source terms [2], whereas the projection of particle properties on to the computational grid and the associated error is still an issue. The spectral projection method allows to compute the continuous field properties with a high precision depending only on the number of Fourier modes. This method has the advantage, compared with the conventional projection methods, to be less sensitive to sampling issues (the number of particles per grid cell).

The method can easily be extended to the computation of different correlation functions. However, only particle number weighted properties can be computed so that the computation of velocity correlations is not possible, whereas momentum autocorrelations can be computed.

The paper is structured as follows. First, the spectral projection method to obtain the Fourier modes is presented. Then, the computation of the autocorrelations is presented. As an example, the method is applied to the case of one million particles subject to the drag force of a decreasing homogeneous isotropic turbulence. The Stokes number is chosen to be $St = 1.57$ based on the dissipative time scale ($\tau^+ = k/\varepsilon$). Then the possibility to determine the implicit filter corresponding to the projection method, and therefore the corresponding error, is demonstrated on the test case. Finally, the features of the method are discussed according to the example.

THE SPECTRAL PROJECTION METHOD

DPS and related methods usually track a large number (N) of individual particles and their properties. Therefore, the location $\mathbf{X}^{(n)}$ of a particle (n) as well as its velocity components U, V, W (or $V_i^{(n)}$) and other properties such as diameter $d^{(n)}$ or temperature $T^{(n)}$ are known.

In many applications, the property of the individual particle is however unimportant compared with the collective properties of particles in that region. In an internal combustion engine, for example, one would be interested in the droplet concentration in the vicinity of the spark plug and the average droplet diameter but not in the diameter of every individual particle. In DPS, the collective properties of particles are usually determined by some kind of projection method.

DOI: 10.1002/fld

Common projection methods

It is common practice to define a particle number density using the following expression that arises in cases of ensemble averaging [3]:

$$n_p(\mathbf{x}) = \sum_n \delta(\mathbf{x} - \mathbf{X}^{(n)}) \tag{1}$$

Owing to the discrete nature of the particle when regarded as a point, a countable infinite number of particles is not sufficient to create a continuous function for the particle number density. Furthermore, the grid of the carrier phase always has a fixed cell size. Therefore, the particles are projected on to the grid using some kind of projection operator (also called local volume averaging) with a characteristic length scale Δ instead of the dirac delta function:

$$\tilde{n}_p(\mathbf{x}) = \sum_n F_\Delta(\mathbf{x} - \mathbf{X}^{(n)}) \tag{2}$$

In the most simple procedure, the particles in a cell are simply added for the discretization, resulting in a particle density of cell (m):

$$\bar{n}_p(m) = \sum_n f^{(m)}(\mathbf{X}^{(n)}) \tag{3}$$

Here, the function $f^{(m)}$ is simply 1 if $X^{(n)}$ is in the cell (m) and 0 otherwise.

The spectral projection method for the number density

The idea of the spectral projection method is rather simple. Assume that we have the number density with an arbitrary projection operator g (which may also be the dirac function). Then the number density can be defined as

$$n_p(\mathbf{x}) = \sum_n g(\mathbf{x} - \mathbf{X}^{(n)}) \tag{4}$$

The Fourier transform $\mathscr{F}$ of the projection operator is

$$\mathscr{F}(g(\mathbf{x} - \mathbf{X}^{(n)})) = \frac{1}{(2\pi)^{3/2}} \int g(\mathbf{x} - \mathbf{X}^{(n)}) \mathrm{e}^{-\mathrm{i}\mathbf{k}\mathbf{x}} \, \mathrm{d}x = \mathrm{e}^{-\mathrm{i}\mathbf{k}\mathbf{X}^{(n)}} \hat{g}(\mathbf{k}) \tag{5}$$

Then this allows to easily define the Fourier transform of the number density (Equation (1)) as

$$\hat{n}_p(\mathbf{k}) = \mathscr{F}(n_p(\mathbf{x})) = \sum_n \mathrm{e}^{-\mathrm{i}\mathbf{k}\mathbf{X}^{(n)}} \hat{g}(\mathbf{k}) \tag{6}$$

Using the dirac delta function for g as the projection operator leads to the convenient formula for the spectral number density (Equation (7)), which can be easily implemented. It is important to note that the use of the dirac function as a projection operator allows a projection without a filter or a characteristic length scale. The implicit spectral filter is given by the number of Fourier modes used for the spectral discretization:

$$\hat{n}_p(\mathbf{k}) = \sum_n (\cos(\mathbf{k}\mathbf{X}^{(n)}) - \mathrm{i}\sin(\mathbf{k}\mathbf{X}^{(n)}))^{\ddagger} \tag{7}$$

[‡]A sketch of the very simple numerical algorithm and cost is given in Appendix A.

DOI: 10.1002/fld

As the spectral number density is computed as the sum over sine and cosine of all particle locations, the numerical effort is proportional to the chosen spectral resolution times the number of particles considered. This sum can, however, easily be parallelized with different strategies.

The Fourier transform of the particle momentum can be obtained in analogy to the particle number density as follows:

$$\mathscr{F}(n_p u_{p,i}(\mathbf{x})) = \widehat{n_p u_{p,i}}(\mathbf{k}) = \sum_n V_i^{(n)} \mathrm{e}^{-\mathrm{i}\mathbf{k}\mathbf{X}^{(n)}} \tag{8}$$

As in the case of the Fourier transform of the particle number density, the computation is simply performed by the sum of cosines and sines of the particle location multiplied by the particle velocity at the location.

COMPUTATION OF POWER SPECTRUM AND AUTOCORRELATION FUNCTION

When particles undergo the forces of a turbulent carrier phase they tend, depending on the relative Stokes number, to accumulate in regions of high strain and low vorticity [1]. This preferential concentration of particles can be studied using the radial distribution function $g(r)$. One difficulty is the computation of this property. Février [3] proposes the following approach described in Equation (10). For this, he introduces the averaging operator $\langle . \rangle = \int . \mathrm{d}\mathbf{x}$ as the volume average over the computational domain. The two-particle distribution function $n_{pp}(\mathbf{x}, \mathbf{x}+\mathbf{r})$ is then defined by Février as

$$n_{pp}(\mathbf{x}, \mathbf{x}+\mathbf{r}) = \sum_{n,m,n\neq m} \delta(\mathbf{x}-\mathbf{X}^{(n)}) \delta(\mathbf{x}+\mathbf{r}-\mathbf{X}^{(m)}) \tag{9}$$

The radial distribution function is then defined by

$$g(\mathbf{r}) = \frac{\langle n_{pp}(\mathbf{x}, \mathbf{x}+\mathbf{r}) \rangle}{\langle n_p(\mathbf{x}) \rangle \langle n_p(\mathbf{x}+\mathbf{r}) \rangle} \tag{10}$$

A physical interpretation of the radial distribution function $g(r)$ is the normalized number of particle centres located in spherical shell of radius $\mathbf{r}$ and $\mathbf{r}+d\mathbf{r}$ about a central particle. It allows therefore to study the structure of the regions of high particle concentrations. In simulations with particle collisions, this quantity can be used to study the effect of preferential concentration on collision rates [1].

The two-particle radial distribution functions with spectral projection

Once the spectral number density (Equation (6)) is computed, it can be used to compute the space-averaged two-particle distribution function with Equation (11). A mathematical derivation of this equation is given in Appendix A:

$$\int n_{pp}(\mathbf{x}, \mathbf{x}+\mathbf{r}) \, \mathrm{d}\mathbf{x} = \frac{1}{(2\pi)^3} \mathscr{F}^{-1}(\hat{n}_p(\mathbf{k}) \hat{n}_p(-\mathbf{k})) - N\delta(\mathbf{r}) \tag{11}$$

DOI: 10.1002/fld

Here, N is the number of discrete particles used for the computation. Then the radial distribution function can simply be expressed by

$$g(\mathbf{r}) = \frac{1}{(2\pi)^3}\frac{1}{N^2}\mathscr{F}^{-1}(\hat{n}_p(\mathbf{k})\hat{n}_p(-\mathbf{k})) - \frac{1}{N}\delta(\mathbf{r}) \tag{12}$$

The two-particle radial distribution function contains the difference between two dirac functions. As, in practical computations, always a finite number of Fourier modes are used to compute $\hat{n}_p(\mathbf{k})$; the dirac function can be subtracted when using the spectral representation of the dirac function with the same number of Fourier modes.

Momentum autocorrelation functions

For the study of turbulence, it is common practice to look at the autocorrelation functions and the kinetic energy spectra. As most of the studies concern incompressible turbulence, the common definition for autocorrelation functions ignores the density of the fluid [4, 5].

$$\begin{aligned} \tilde{\mathscr{R}}_{ij}(\mathbf{r}) &= \int u_i(\mathbf{x})u_j(\mathbf{x}+\mathbf{r})\,\mathrm{d}\mathbf{x} \\ \mathscr{R}_{ij}(\mathbf{r}) &= \tilde{\mathscr{R}}_{ik}^{-1}(0)\tilde{\mathscr{R}}_{kj}(\mathbf{r}) \end{aligned} \tag{13}$$

For a discrete particle, the autocorrelation function can be defined [3, 6] using the conditional statistical averaging operator $\langle|\rangle$ as

$$\tilde{\mathscr{R}}_{ij}^{pp}(\mathbf{r}) = \langle V_i^{(n)} V_j^{(m)} | \mathbf{x} = \mathbf{X}^{(n)}\mathbf{x} + \mathbf{r} = \mathbf{X}^{(m)} | m \neq n \rangle \tag{14}$$

In the same manner as the two-particle radial distribution function, the momentum autocorrelation function can be expressed in terms of the Fourier transformed of the particle momentum:

$$\tilde{\mathscr{R}}_{ij}^{pp}(\mathbf{r}) = \frac{1}{(2\pi)^3}\mathscr{F}^{-1}(n_p u_{p,i}(\mathbf{k}) n_p u_{p,j}(-\mathbf{k})) - \delta(\mathbf{r})\sum_n V_i^{(n)} V_j^{(n)} \tag{15}$$

Proof is given in Appendix A. As in the definition of the autocorrelation of the carrier phase, it is common practice to define the normalized autocorrelation function for the particle momentum as given in the following equation:

$$\mathscr{R}_{ij}^{pp}(\mathbf{r}) = \tilde{\mathscr{R}}_{ik}^{pp-1}(0)\tilde{\mathscr{R}}_{kj}^{pp}(\mathbf{r}) \tag{16}$$

It is important that here $\mathscr{R}_{ij}^{pp}$ is a momentum and not a velocity autocorrelation. In the case of an incompressible fluid the expressions are identical. In the case of a compressible fluid the density, or as in the present case of the spectral projection method the number density, enters this expression and cannot be separated.

APPLICATION TO THE TEST CASE

In this section, the proposed method is applied to the test case of undistinguishable point particles. In the first test case, the particles are randomly distributed in space and in the second test the particles are subject to the Stokes drag force in decaying homogeneous isotropic turbulence.

DOI: 10.1002/fld

In the second test case, the carrier phase was initialized with an incompressible velocity field of a Passot Pouquet spectrum. After one eddy turnover time, particles were added and the computation was continued for an additional eddy turnover time. The low Reynolds number of $Re = 13.6$ was chosen with respect to the spatial resolution of the projected particle number densities. The carrier phase grid resolution is (64^3). Particle Stokes number at the injection time is $St = 1.57$ based on the particle relaxation time scale and the dissipative time scale ($\tau^+ = k/\varepsilon$) of the flow. Collisions are not considered. The particles show significant effects of preferential concentration.

The necessary spectral resolution and the dirac function

The necessary number of Fourier components depends, as in a usual grid projection, on the number of projected components. The difference is the absence of a filter in the case of a spectral projection. One difficulty associated with the computation of the autocorrelation functions is the existence of a dirac function in the formula. One way of solving the problem is to use the numerical representation of the dirac function. A dirac function can mathematically be represented as

$$\delta(r) = \int \mathrm{e}^{\mathrm{i}kr}\,\mathrm{d}k \tag{17}$$

The numerical representation with the equivalent number of nodes is just the inverse Fourier transform with the number of nodes of the constant function $\hat{f}(k) = 1$:

$$\delta(r)_N = \mathscr{F}_N^{-1}\{1\} \tag{18}$$

Of course, there is also an analytical expression for the spatial coefficients. The numerical representation of the dirac function is shown in Figure 1. The spatial resolution for which point projection method is exact is roughly π/N for a box of size 2π and N Fourier modes for every space direction. This roughly corresponds to the width of the dirac function as shown in Figure 1 as well. All

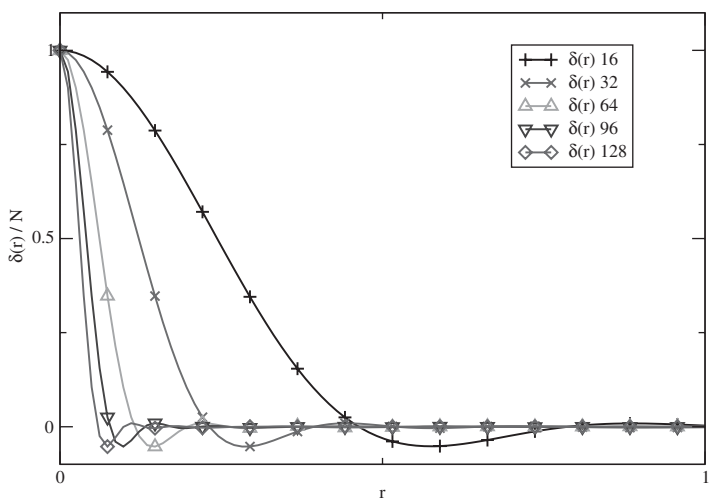

Figure 1. Numerical representation of the one-dimensional dirac function $\delta(r)$ with different numbers of Fourier components.

DOI: 10.1002/fld

projections have been computed on a desktop PC and are therefore limited to a resolution of 128 Fourier modes per space direction.

The radial distribution function

The radial distribution function $g(r)$ of randomly distributed particles is by definition equal to unity ($g(r)=1$). The convergence of the method can therefore be studied easily with random particles. For this case test, fields with 10, 100, 1000, 10 000 and 100 000 randomly spaced particles in 2π periodic box were analysed with 16 Fourier components by space direction. The radial distribution function is shown in Figure 2. The convergence of the radial distribution function in terms of particle number can be easily explained by considering the sampling theorem. The critical number is two points per cycle; an interpolation with $16^3=4096$ therefore requires at least 8192 points. Therefore, the radial distribution function with 10 000 particles is almost converged and equal to unity for 100 000 particles.

For the test case of particles in homogeneous turbulence, the radial distribution functions $g(r)$ obtained with different total numbers of Fourier components are shown in Figure 3. The spatial segregation is strong and one can see how $g(r)$ does not converge as the number of Fourier modes is increased up to 128 per space direction. Such a behaviour is typically observed when standard volume filtering techniques are used [3].

The spectral projection allows us to evaluate the spatial resolution accuracy of the field. As the Fourier components obtained by the spectral projection method are exact and do not undergo a filtering procedure, the magnitude of the Fourier components can be used to check whether the spatial resolution of the field is sufficient. This can be applied to a later computation in an Eulerian framework or in an analysis in a Lagrangian framework. Figure 4 shows the norm of the Fourier coefficients associated with the particle number density for the test case of $St=1.57$. It can be seen that up to a large Fourier number and thus to a small physical scale, the number density field undergoes strong changes, so that the radial distribution function in physical space

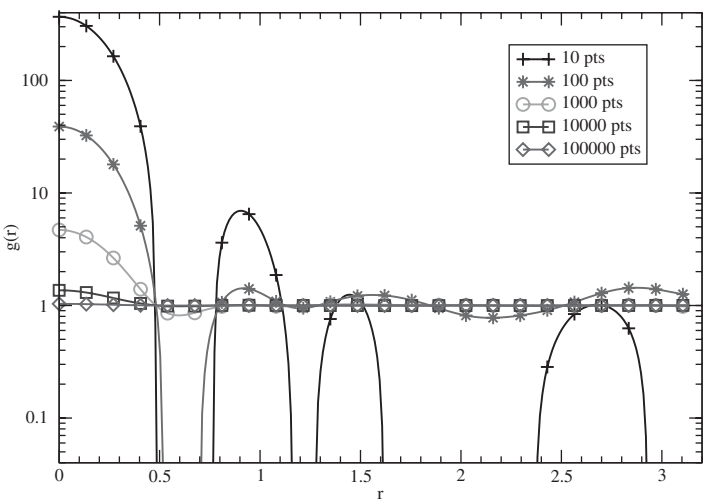

Figure 2. The radial distribution function $g(r)$ for randomly distributed particles.

DOI: 10.1002/fld

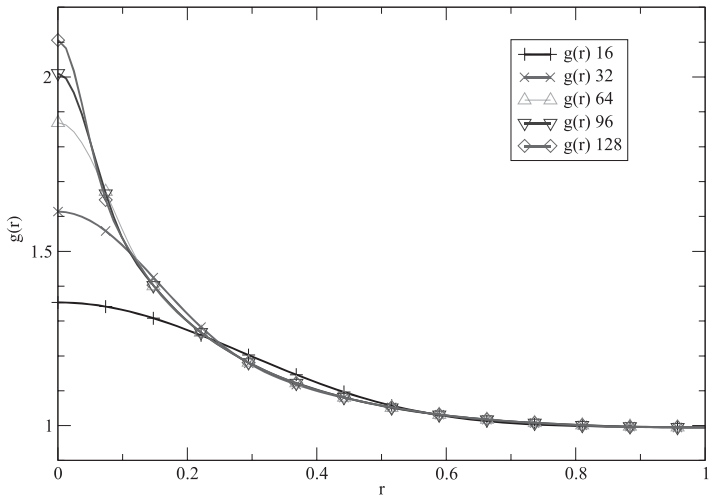

Figure 3. The radial distribution function $g(r)$ for different numbers of Fourier coefficients per space direction in the case of $St = 1.57$.

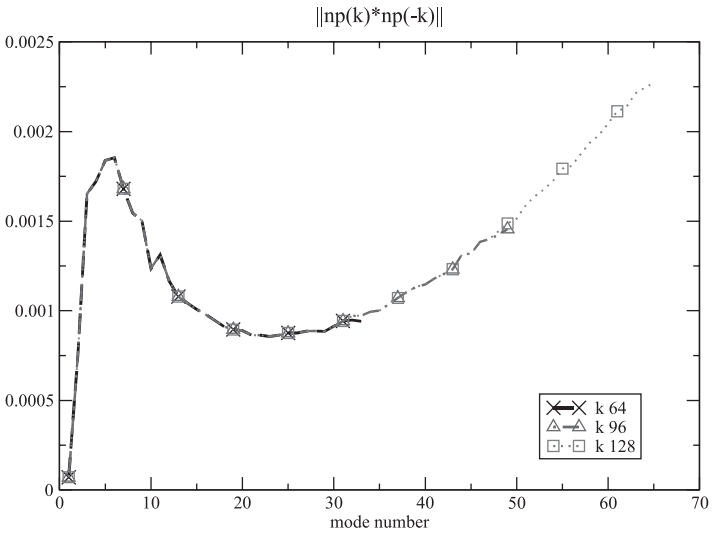

Figure 4. Norm of the Fourier components with a different number of Fourier modes for the test case of $St = 1.57$.

does not converge (see Figure 3). Figures 5 and 6 show the norm of the Fourier coefficients associated with the particle number density for a different number of particles. In the case of randomly distributed particles, the norm just increases as higher-frequency components are needed to represent the particles. This becomes clear if one thinks of the particles as a finite sum of dirac functions at different space locations. The figures show that a small number of particles lead to the Fourier components of increasing magnitude for a higher mode number. As the number of

DOI: 10.1002/fld

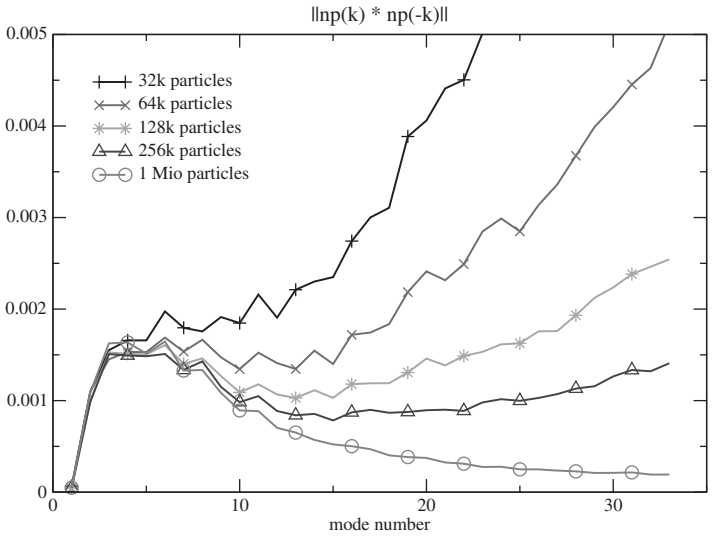

Figure 5. Norm of the Fourier components with a different number of particles for the test case of $St = 1.57$.

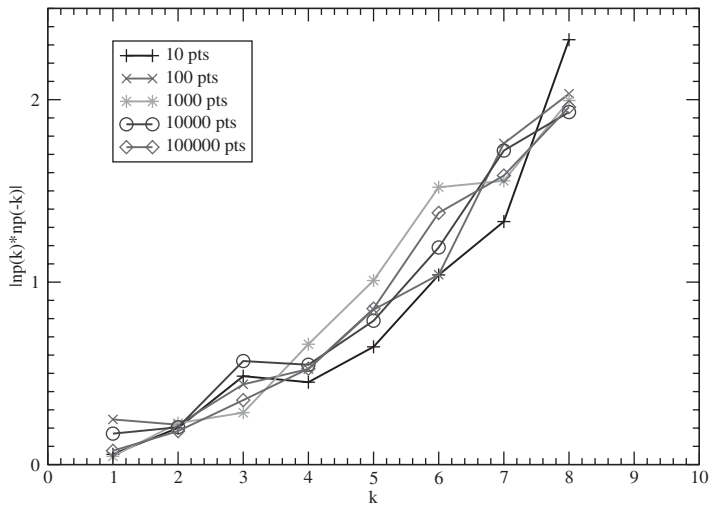

Figure 6. Norm of the Fourier components with a different number of particles for test case of randomly distributed particles and 16 Fourier components per space direction.

particles increases in the case of homogeneous turbulence, the corresponding density field becomes more and more *smooth* and the magnitude of the Fourier components converges. The norm of the Fourier components however does not decrease like the kinetic energy in homogeneous turbulence. This is due to the fact the the energy of small eddies is much smaller than the energy of large

DOI: 10.1002/fld

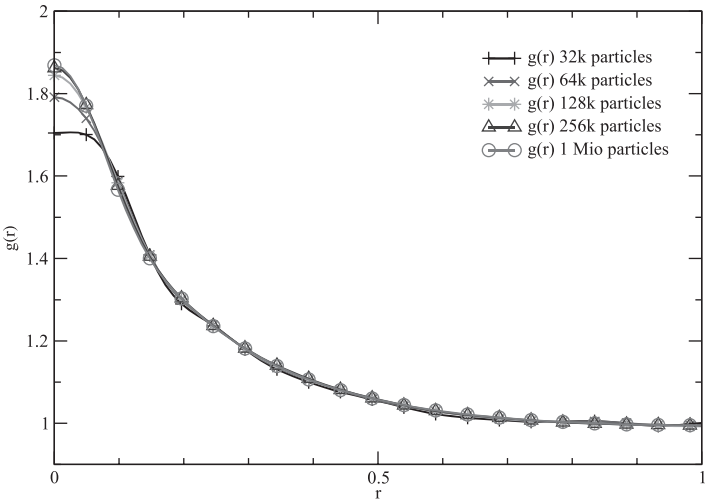

Figure 7. $g(r)$ of case $St = 1.57$ with different particle numbers for the spectral projection method and 64 Fourier modes.

eddies. The fluctuating component of the particle increases however if one goes to smaller scales and thus the magnitude of the Fourier components increases.

In both Figures 3 and 4, the function $g(r)$ converges down to a length scale of roughly $2\pi/N$. For a convergence down to a smaller length scale, more Fourier coefficients are required. The convergence in terms of particle number is shown in Figure 7. It can be seen that for the present case a particle number (256k) corresponding roughly to the total number of Fourier modes (64^3) is sufficient for a reasonable convergence of the particle autocorrelation function $g(r)$.

The momentum autocorrelation functions

For the case of Stokes number $St = 1.57$, the momentum autocorrelation functions are shown in Figure 8. For a comparison, the velocity autocorrelations of the carrier phase at the same moment are shown in Figure 9. The significant steeper behaviour of the particle momentum correlations at the origin can however not be interpreted directly as a smaller 'microscale' as the particle concentration is intrinsingly coupled to this quantity. $g(r)$ indeed shows a significant rise at the origin (Figure 3) and therefore effects the momentum autocorrelation.

COMPUTATION OF THE FILTER CORRESPONDING TO A PROJECTION METHOD

As the spectral computation does not contain a filter other than the cut-off in Fourier components at the chosen precision, this method can be used to compute the filter function corresponding to the projection method. A filtered field $\tilde{f}$ is usually obtained by a convolution of the original field f with a filter G in real space:

$$\tilde{f}(x) = \int f(x')G(x'-x)\,\mathrm{d}x' \tag{19}$$

DOI: 10.1002/fld

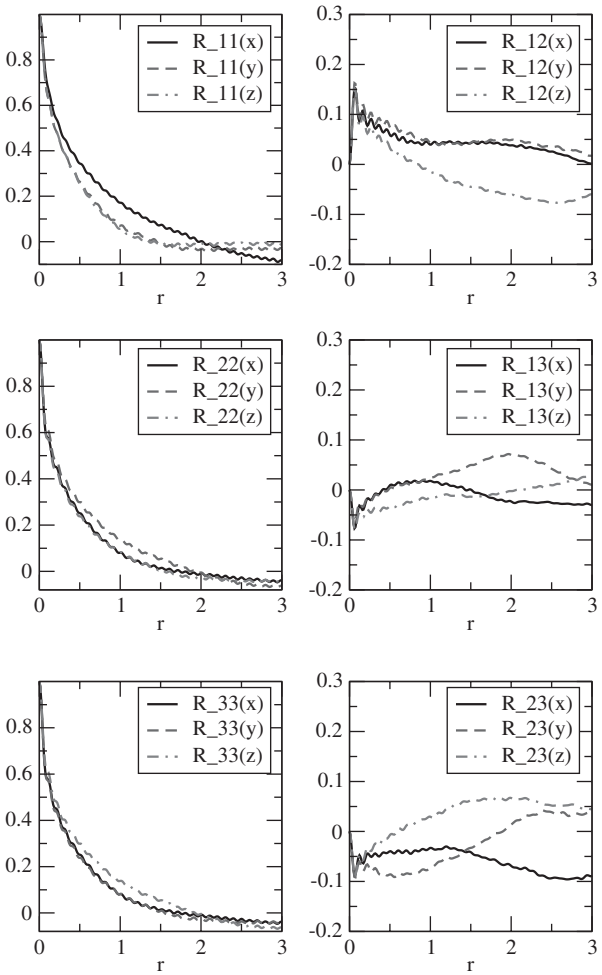

Figure 8. The momentum autocorrelation functions obtained with the spectral projection method for the test case $St = 1.57$ after two eddy turnover times.

Using the properties of the Fourier transform, the convolution product becomes a simple product in spectral space:

$$\hat{\bar{f}}(k) = \hat{f}(k)\hat{G}(k) \tag{20}$$

This allows to compute the spectral filter function by

$$\hat{G}(k) = \hat{\bar{f}}(k)/\hat{f}(k) \tag{21}$$

This method can be applied to the number density field to obtain the implicit filter of a projection method on a grid of given precision. As an example, this method is applied to the test case with the particles of a Stokes number of $St = 1.57$ on a spatial grid of 64^3. Equation (21) is used to

DOI: 10.1002/fld

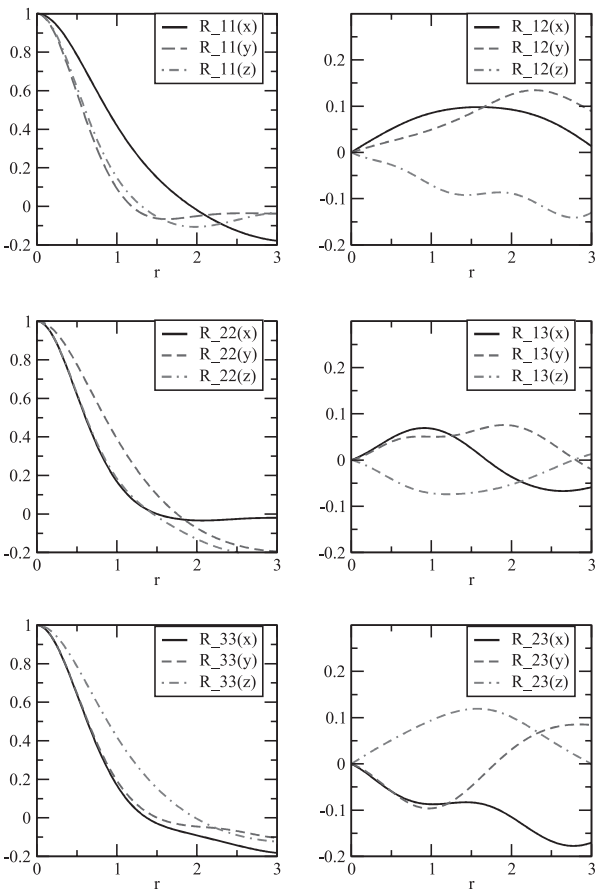

Figure 9. The velocity autocorrelation function of the carrier phase after two eddy turnover times.

determine $G(k)$. As G is assumed isotropic in space, Figure 10 shows the magnitude of the Fourier coefficients over k. The number density was obtained using a Gaussian filter. It can be seen that this high-quality filter preserves the first 10 modes of the original solution. The corresponding real-space filter is shown in Figure 11. It shows that the projection method almost behaves like a dirac on the field and only the two neighbouring cells receive a small amount of the component. This simple computation of the implicit filter shows how the spectral projection method can be used to determine the quality of a projection method used in a fluid mechanics code projecting source terms and particle properties on a Eulerian grid.

THE ISSUE OF NEGATIVE NUMBER DENSITIES

The backward Fourier transform of the spectral projected quantities allows to determine the values of number densities and momentum in physical space. As the spectral projection method delivers a truncated series of Fourier components of the interpolation of a series of dirac functions, it

DOI: 10.1002/fld

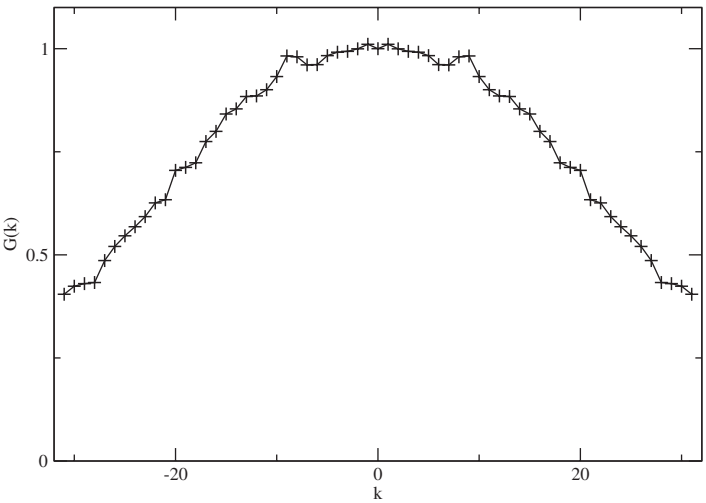

Figure 10. Spectral filter $\|G(k)\|$ obtained with Equation (21) from a Gaussian-projected field [7] and the spectral-projected field.

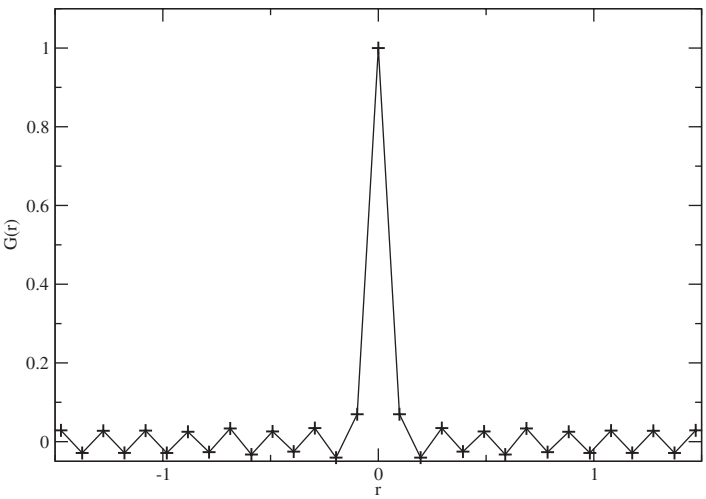

Figure 11. Real filter $G(r)$ obtained with Equation (21) from a Gaussian-projected field [7] and the spectral-projected field.

inevitably shows at some locations such things as negative number densities. This can easily be illustrated by considering the truncated dirac function in Figure 1. The dirac function computed with a truncated series of Fourier components always admits a negative loop next to the origin. For a single particle located at the origin, the dirac function would represent the number density field. If one displaces the numerical representation of the dirac function to the particle locations

DOI: 10.1002/fld

and computes the sum of those dirac functions, one obtains the number density field with small negative loops next to the location of every particle. The Fourier components are mathematically exact but are in numerical applications always a truncated series of the entire expression. As the spectral representation of space dirac function is 1 at all wave numbers, this series does not converge.

If one insists on using the spectral projected quantities to produce the number densities and momentum in real space, attenuation factors can be used to make the series converge [8]. This corresponds however to the introduction of a filter function in spectral space. As an example, a cut of the $z=0$ plane of the computation is given in Figure 12 for a Gaussian and a spectral projection. The filter of the Gaussian projection corresponds to the filter computed in the section. It can be seen that the spectral projection method allows for negative components, whereas the Gaussian projection method is at least 0. On the other hand, it is visible to what degree the Gaussian method does smooth out small changes in the number density.

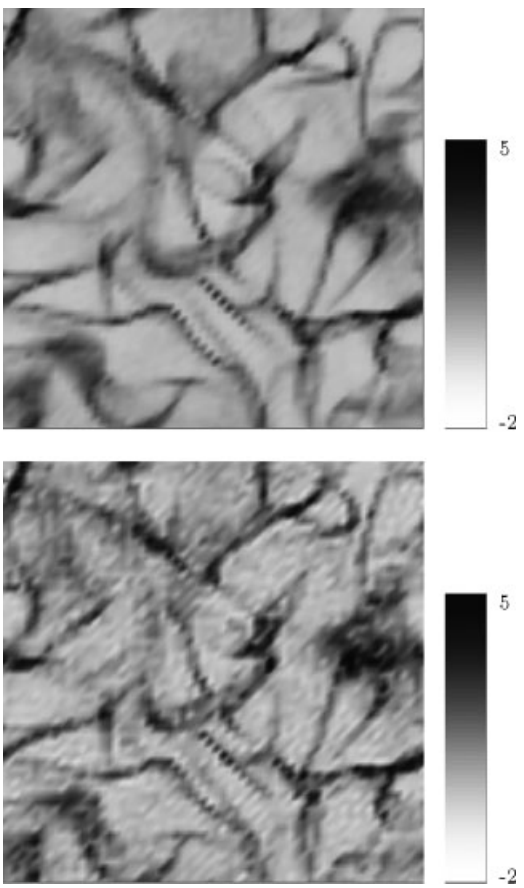

Figure 12. The normalized number density fields obtained by a Gaussian-projection method (top) and with backward Fourier transform from the spectral projection method (bottom) after two eddy turnover times for a Stokes number of $St=1.57$.

DOI: 10.1002/fld

CONCLUSION

Owing to the numerical cost and the geometric limitation in physical space, the spectral projection method is not a tool that can be used in the two-phase flow computation in complex geometries. It is not suited to compute a projection on the carrier phase for the evaluation of source terms. It is however a tool that can be used to qualify the numerical tool in question and to analyse the error limits that are often not known. Especially, the computation of the numerical filter associated with a certain method should be useful at this point. It allows to analyse the precision of academic and commercial two-phase flow tools *a posteriori*. Furthermore, we feel that the computation of autocorrelation functions is significantly improved with the presented method as there is no direct introduction of a filter by the projection method on the computational grid. Owing to simplicity of the method (sine and cosine functions of particle location), this method is very easy and fast to implement. The numerical examples of particles in decaying homogeneous isotropic turbulence are not exhaustive. They are only to be considered as an example of the ease of application and to demonstrate the potential of the method.

APPENDIX A

Computation of the two-particle distribution function

$$
\begin{aligned}
\langle n_{pp}(\mathbf{x},\mathbf{x}+\mathbf{r})\rangle &= \int n_{pp}(\mathbf{x},\mathbf{x}+\mathbf{r})\,\mathrm{d}\mathbf{x}\\
&= \int \sum_{n,m,n\neq m} \delta(\mathbf{x}-\mathbf{X}^{(n)})\delta(\mathbf{x}+\mathbf{r}-\mathbf{X}^{(m)})\,\mathrm{d}\mathbf{x}\\
&= \sum_{n,m,n\neq m} \frac{1}{(2\pi)^6}\int\!\!\int\!\!\int \mathrm{e}^{\mathrm{i}\mathbf{k}(\mathbf{x}-\mathbf{X}^{(n)})}\mathrm{e}^{\mathrm{i}\tilde{\mathbf{k}}(\mathbf{x}+\mathbf{r}-\mathbf{X}^{(m)})}\,\mathrm{d}\mathbf{k}\,\mathrm{d}\tilde{\mathbf{k}}\,\mathrm{d}\mathbf{x}\\
&= \sum_{n,m,n\neq m} \frac{1}{(2\pi)^6}\int\!\!\int\!\!\int \mathrm{e}^{\mathrm{i}(\mathbf{k}+\tilde{\mathbf{k}})\mathbf{x}}\mathrm{e}^{\mathrm{i}\mathbf{k}\mathbf{r}}\mathrm{e}^{-\mathrm{i}\mathbf{k}(\mathbf{X}^{(n)})}\mathrm{e}^{-\mathrm{i}\tilde{\mathbf{k}}(\mathbf{X}^{(m)})}\,\mathrm{d}\mathbf{k}\,\mathrm{d}\tilde{\mathbf{k}}\,\mathrm{d}\mathbf{x}\\
&= \sum_{n,m,n\neq m} \frac{1}{(2\pi)^3}\int\!\!\int \delta(\mathbf{k}+\tilde{\mathbf{k}})\mathrm{e}^{\mathrm{i}\mathbf{k}\mathbf{r}}\mathrm{e}^{-\mathrm{i}\mathbf{k}(\mathbf{X}^{(n)})}\mathrm{e}^{-\mathrm{i}\tilde{\mathbf{k}}(\mathbf{X}^{(m)})}\,\mathrm{d}\mathbf{k}\,\mathrm{d}\tilde{\mathbf{k}}\\
&= \frac{1}{(2\pi)^3}\sum_{n,m,n\neq m}\int \mathrm{e}^{-\mathrm{i}\mathbf{k}\mathbf{r}}\mathrm{e}^{\mathrm{i}\mathbf{k}\mathbf{X}^{(n)}}\mathrm{e}^{-\mathrm{i}\mathbf{k}\mathbf{X}^{(m)}}\,\mathrm{d}\mathbf{k}\\
&= \frac{1}{(2\pi)^3}\sum_{n,m}\int \mathrm{e}^{-\mathrm{i}\mathbf{k}\mathbf{r}}\mathrm{e}^{-\mathrm{i}\mathbf{k}(\mathbf{X}^{(n)})}\mathrm{e}^{\mathrm{i}\mathbf{k}\mathbf{X}^{(m)}}\,\mathrm{d}\mathbf{k} - \frac{1}{(2\pi)^3}\sum_{n}\int \mathrm{e}^{-\mathrm{i}\mathbf{k}\mathbf{r}}\mathrm{e}^{\mathrm{i}\mathbf{k}\mathbf{X}^{(n)}}\mathrm{e}^{-\mathrm{i}\mathbf{k}\mathbf{X}^{(n)}}\,\mathrm{d}\mathbf{k}\\
&= \frac{1}{(2\pi)^3}\int \mathrm{e}^{-\mathrm{i}\mathbf{k}\mathbf{r}}\left(\sum_n \mathrm{e}^{-\mathrm{i}\mathbf{k}\mathbf{X}^{(n)}}\right)\left(\sum_m \mathrm{e}^{\mathrm{i}\mathbf{k}\mathbf{X}^{(m)}}\right)\mathrm{d}\mathbf{k} - \frac{1}{(2\pi)^3}\sum_n\int \mathrm{e}^{-\mathrm{i}\mathbf{k}\mathbf{r}}\,\mathrm{d}\mathbf{k}\\
&= \frac{1}{(2\pi)^3}\mathscr{F}^{-1}(\hat{n}_p(\mathbf{k})\hat{n}_p(-\mathbf{k})) - N\delta(\mathbf{r}) \qquad \text{(A1)}
\end{aligned}
$$

DOI: 10.1002/fld

Computation of momentum autocorrelation

$$
\begin{aligned}
\tilde{\mathscr{R}}_{ij}^{pp}(\mathbf{r}) &= \int \sum_{n,m,n\neq m} V_i^{(n)} \delta(\mathbf{x}-\mathbf{X}^{(n)}) V_j^{(m)} \delta(\mathbf{x}+\mathbf{r}-\mathbf{X}^{(m)})\,\mathrm{d}\mathbf{x} \\
&= \sum_{n,m,n\neq m} \frac{1}{(2\pi)^6} \iiint V_i^{(n)} V_j^{(m)} \mathrm{e}^{\mathrm{i}\mathbf{k}(\mathbf{x}-\mathbf{X}^{(n)})} \mathrm{e}^{\mathrm{i}\tilde{\mathbf{k}}(\mathbf{x}+\mathbf{r}-\mathbf{X}^{(m)})}\,\mathrm{d}\mathbf{k}\,\mathrm{d}\tilde{\mathbf{k}}\,\mathrm{d}\mathbf{x} \\
&= \sum_{n,m,n\neq m} \frac{1}{(2\pi)^6} \iiint V_i^{(n)} V_j^{(m)} \mathrm{e}^{\mathrm{i}(\mathbf{k}+\tilde{\mathbf{k}})\mathbf{x}} \mathrm{e}^{\mathrm{i}\mathbf{k}\mathbf{r}} \mathrm{e}^{-\mathrm{i}\mathbf{k}(\mathbf{X}^{(n)})} \mathrm{e}^{-\mathrm{i}\tilde{\mathbf{k}}(\mathbf{X}^{(m)})}\,\mathrm{d}\mathbf{k}\,\mathrm{d}\tilde{\mathbf{k}}\,\mathrm{d}\mathbf{x} \\
&= \sum_{n,m,n\neq m} \frac{1}{(2\pi)^3} \iint V_i^{(n)} V_j^{(m)} \delta(\mathbf{k}+\tilde{\mathbf{k}}) \mathrm{e}^{\mathrm{i}\mathbf{k}\mathbf{r}} \mathrm{e}^{-\mathrm{i}\mathbf{k}(\mathbf{X}^{(n)})} \mathrm{e}^{-\mathrm{i}\tilde{\mathbf{k}}(\mathbf{X}^{(m)})}\,\mathrm{d}\mathbf{k}\,\mathrm{d}\tilde{\mathbf{k}} \\
&= \frac{1}{(2\pi)^3} \sum_{n,m,n\neq m} \int V_i^{(n)} V_j^{(m)} \mathrm{e}^{-\mathrm{i}\mathbf{k}\mathbf{r}} \mathrm{e}^{\mathrm{i}\mathbf{k}\mathbf{X}^{(n)}} \mathrm{e}^{-\mathrm{i}\mathbf{k}\mathbf{X}^{(m)}}\,\mathrm{d}\mathbf{k} \\
&= \frac{1}{(2\pi)^3} \sum_{n,m} \int V_i^{(n)} V_j^{(m)} \mathrm{e}^{-\mathrm{i}\mathbf{k}\mathbf{r}} \mathrm{e}^{-\mathrm{i}\mathbf{k}(\mathbf{X}^{(n)})} \mathrm{e}^{\mathrm{i}\mathbf{k}\mathbf{X}^{(m)}}\,\mathrm{d}\mathbf{k} - \frac{1}{(2\pi)^3} \\
&\quad \times \sum_{n} \int V_i^{(n)} V_j^{(n)} \mathrm{e}^{-\mathrm{i}\mathbf{k}\mathbf{r}} \mathrm{e}^{\mathrm{i}\mathbf{k}\mathbf{X}^{(n)}} \mathrm{e}^{-\mathrm{i}\mathbf{k}\mathbf{X}^{(n)}}\,\mathrm{d}\mathbf{k} \\
&= \frac{1}{(2\pi)^3} \int \mathrm{e}^{-\mathrm{i}\mathbf{k}\mathbf{r}} \left(\sum_n V_i^{(n)} \mathrm{e}^{-\mathrm{i}\mathbf{k}\mathbf{X}^{(n)}} \right) \left(\sum_m V_j^{(m)} \mathrm{e}^{\mathrm{i}\mathbf{k}\mathbf{X}^{(m)}} \right) \mathrm{d}\mathbf{k} - \frac{1}{(2\pi)^3} \sum_n V_i^{(n)} V_j^{(n)} \int \mathrm{e}^{-\mathrm{i}\mathbf{k}\mathbf{r}}\,\mathrm{d}\mathbf{k} \\
&= \frac{1}{(2\pi)^3} \mathscr{F}^{-1}(n_p u_{p,i}(\mathbf{k}) n_p u_{p,j}(-\mathbf{k})) - \delta(\mathbf{r}) \sum_n V_i^{(n)} V_j^{(n)}
\end{aligned}
\tag{A2}
$$

Sketch of the numerical algorithm

A numerical implementation in pseudo-code for the computation of the spectral projection of the particles is given below.

```
/* N_part is the number of particles            */
/* Nx,Ny,Nz are the number of fourier components */

/* variables for particle locations             */
double x_p[N_part],y_p[N_part],z_p[N_part];

/* variables for discrete fourier transformed   */
/* of the particle density field                */
double np_real[Nx*Ny*Nz];
double np_imag[Nx*Ny*Nz];

long  double sum_sin,sum_cos;
int   j,kx,ky,kz;
```


DOI: 10.1002/fld

```
/* computation of the discrete fourier transform */
for(kx=-Nx/2;kx<Nx/2;kx++)
 for(ky=-Ny/2;ky<Ny/2;ky++)
  for(kz=-Nz/2;kz<Nz/2;kz++)
  {
   sum_cos = 0.0;
   sum_sin = 0.0;
   for(j=0;j<N_part;j++)
   {
    sum_cos = sum_cos +
              cos(kx*x_p[j]+ky*y_p[j]+kz*z_p[j]);
    sum_sin = sum_sin +
              sin(kx*x_p[j]+ky*y_p[j]+kz*z_p[j]);
   }

   np_real[(kx+Nx/2)+(ky+Ny/2)*(Nx)+(kz+Nz/2)*(Nx*Ny)] = sum_cos;
   np_imag[(kx+Nx/2)+(ky+Ny/2)*(Nx)+(kz+Nz/2)*(Nx*Ny)] = sum_sin;
  }
```

The cost for the computation of the discrete Fourier transform of the number density field can easily be computed to be proportional to $N_x * N_y * N_z * N_{\text{part}}$. In comparison, a fast Fourier transform of a number density field is proportional to $N * \log(N)$.

The numerical cost for the computation of $g(r)$ is then proportional to $N_x * N_y * N_z * N_{\text{loc}}$, where N_{loc} is the number of locations of evaluations of $g(r)$ at the distance r. Therefore, the dominant cost lies in the evaluation of the discrete Fourier transform at the particle locations.

REFERENCES

1. Reade WC, Collins LR. Effect of preferential concentration on turbulent collision rates. *Physics of Fluids* 2000; **12**(10):2530–2540.
2. Yeung PK, Pope SB. An algorithm for tracking fluid particles in numerical simulations of homogeneous turbulence. *Journal of Computational Physics* 1988; **79**:373–416.
3. Février P. Etude numerique des effets de concentration preferentielle et de correlation spatiale entre vitesses des particules solides en turbulence homogene isotrope stationaire, 2000.
4. Pope SB. Stochastic Lagrangian models of velocity in homogeneous turbulent shear flow. *Physics of Fluids* 2002; **14**(5):1696–1702.
5. Pope SB. *Turbulent Flows*. Cambridge University Press: Cambridge, 2000.
6. Février P, Simonin O, Squires KD. Partitioning of particle velocities in gas–solid turbulent flows into a continuous field and a spatially uncorrelated random distribution: theoretical formalism and numerical study. *Journal of Fluid Mechanics* 2005; **533**:1–46.
7. Kaufmann A, Moreau M, Simonin O, Helie J. Comparison between Lagrangian and mesoscopic Eulerian approaches for inertial particles in decaying isotropic turbulence. *Journal of Computational Physics* 2006; submitted.
8. Gutknecht MH. Attenuation factors in multivariate Fourier analysis. *Numerische Mathematik* 1987; **51**:615–629.

DOI: 10.1002/fld